PIKFYVE inhibition induces endosome- and lysosome-derived vacuole enlargement via ammonium accumulation

Junsuke Uwada [a, *], Hitomi Nakazawa [a], Takeshi Kiyoi [a], Takashi Yazawa [b], Ikunobu Muramatsu [a], Takayoshi Masuoka [a]

[a] Department of Pharmacology, School of Medicine, Kanazawa Medical University, Ishikawa, Japan

[b] Department of Biochemistry, Asahikawa Medical University, Asahikawa 078-8510, Japan

* Corresponding author at:

Junsuke Uwada, PhD

Department of Pharmacology, School of Medicine, Kanazawa Medical University,

1-1 Daigaku, Uchinada, Ishikawa, 920-0293, Japan,

e-mail: uwada@kanazawa-med.ac.jp

Abstract

FYVE-type zinc finger-containing phosphoinositide kinase (PIKFYVE), that is essential for PtdIns(3,5)P_2 production, is an important regulator of lysosomal homeostasis. PIKFYVE dysfunction leads to cytoplasmic vacuolization; however, the underlying mechanism remains unknown. In this study, we explored the cause of vacuole enlargement upon PIKFYVE inhibition in DU145 prostate cancer cell lines. The observed vacuolization was consistent with the localization of endosome and lysosome markers, indicating that the vacuoles were enlarged endosomes and lysosomes. Enlargement of vacuoles by PIKFYVE inhibition required glutamine and its metabolism by glutaminases. Here, addition of ammonia resulted in vacuole enlargement even in the absence of glutamine, suggesting that ammonia generated by glutamine metabolism promotes vacuole enlargement. Moreover, PIKFYVE inhibition led to intracellular ammonium accumulation. Endosome–lysosome permeabilization resulted in ammonia leakage from the cells, indicating ammonia accumulation in the endosomes and lysosomes. Ammonium accumulation and vacuole expansion were suppressed by the lysosomal lumen neutralization. It is therefore assumed that PIKFYVE inhibition interferes with the efflux of NH_4^+, which is protonated NH_3 formed after entering into the lumen, leading to vacuole enlargement due to osmotic swelling. Notably, glutamine or ammonium is required for

PIKFYVE inhibition-induced suppression of lysosomal function and autophagy flux. Over all, this study showed that vacuole enlargement caused by PIKFYVE inhibition was due to the ammonium accumulation in endosomes and lysosomes. Our findings indicate the involvement of PIKFYVE in glutamine–ammonia metabolism and the possibility of pharmacological intervention in glutamine–ammonia metabolism by sequestering ammonia in endosomes and lysosomes.

Keywords

apilimod; cathepsin D; glutaminase; glutamine; PtdIns(3,5)P_2; SB202190; TRPML1; YM201636

Abbreviations

4-PBA: 4-phenylbutyric acid; BAPTA-AM: O,O'-Bis(2-aminophenyl)ethyleneglycol-N,N,N',N'-tetraacetic acid, tetraacetoxymethyl ester; BPTES: bis-2-(5-phenylacetamido-1,3,4-thiadiazol-2-yl) ethyl sulfide; ClC-7: chloride channel 7; ConB: concanamycin B; CQ: chloroquine; DAPI: 4',6-Diamidino-2-phenylindole; EAA: essential amino acids; DMSO: dimethyl sulfoxide; Gln: glutamine; GLS: glutaminase; HBSS: Hanks' balanced salt solution; GI968: glutaminase inhibitor 968; LAMP1: lysosomal-associated

membrane protein 1; LC3: light chain 3; LDH: lactate dehydrogenase; LLOMe: L-leucyl-L-leucine methyl ester; ML-SA1: mucolipin synthetic agonist 1; MP: methyl pyruvate; NAC: N-acetyl-L-cysteine; NEAA: non-essential amino acids; PIKFYVE: FYVE-type zinc finger-containing phosphoinositide kinase; PtdIns(3,5)P_2: Phosphatidylinositol 3,5-bisphosphate; SB: SB202190; SLC12A9: solute carrier family 12 member 9; TRPML1: transient receptor potential mucolipin 1; V-ATPases: vacuolar H^+-ATPases; YM: YM201636; Z-FR-MCA: benzyloxycarbonyl-L-phenylalanyl-L-arginine 4-methylcoumaryl-7-amide

Introduction

Lysosomes are acidic intracellular vesicles containing various hydrolytic enzymes, such as cathepsin, that degrade and recycle biomolecules. Lysosomes degrade materials via endocytosis by fusing with endosomes and contribute to macroautophagy/autophagy-induced degradation by fusing with autophagosomes to form autolysosomes [1]. Lysosomal dysfunction leads to the accumulation of substrates to be degraded, resulting in various pathologies, such as sphingolipidosis and mucopolysaccharidosis [2]. Lysosomal hydrolases are transported to early endosomes via the trans-Golgi network. Early endosomes are converted into late endosomes, which eventually fuse with lysosomes to maintain their function [3]. Vacuolar H^+-ATPases (V-ATPases) localize to the membranes of endosomes and lysosomes and maintain their luminal compartments at an acidic pH. Decreased luminal acidity due to V-ATPase inhibition results in decreased hydrolase activity and reduced autophagic flux [4,5].

Phosphatidylinositol 3,5-bisphosphate (PtdIns(3,5)P_2) is a phosphoinositide specifically localized in endosomes and lysosomes [6]. FYVE-type zinc finger-containing phosphoinositide kinase (PIKFYVE) is an essential kinase for the production of PtdIns(3,5)P_2. PIKFYVE localizes to the membranes of endosomes and lysosomes as a complex with 5-phosphatase FIG4 and scaffolding protein VAC14 and phosphorylates

PtdIns3P [7]. Deletion of PIKFYVE results in the loss of intracellular PtdIns(3,5)P_2 [8]. PIKFYVE plays an important role in lysosomal homeostasis by controlling the reformation of lysosomes [9,10]. PIKFYVE is also required for normal autophagic flux, as it is involved in the formation of autolysosomes via the fusion of lysosomes and autophagosomes [11,12].

PIKFYVE-deficient mice die during embryogenesis [13,14]. Studies on PIKFYVE low-expressing and tissue-specific knockout mice have shown that PIKFYVE is essential for the normal development and function of various tissues [8,14]. *PIKFYVE*-deficient tissues showed abnormally swollen LAMP1-positive vacuoles, suggesting that they are endosomes or lysosomes. Genetic abnormalities in *Fig4* or *Vac14* also reduce PtdIns(3,5)P_2 production, leading to neurodegeneration and enlarged cytoplasmic vacuoles [15,16]. An in vitro study has shown that deficiency in PIKFYVE kinase-mediated PtdIns(3,5)P_2 production leads to characteristic vacuolation [17]. The formation of these vacuoles may be related to dysregulated endosome–lysosome function; however, the underlying mechanism remains unclear. Previous studies have indicated that vacuoles are formed because of an imbalance favoring the lysosomal fusion over fission in the lysosomal fusion and fission process [12,18]. However, whether this abnormality in the lysosomal fusion–fission process was sufficient to explain the vacuole enlargement

induced by PIKFYVE inhibition remains unknown.

In this study, we demonstrated that vacuole enlargement induced by PIKFYVE inhibition requires ammonium produced by glutamine metabolism. PIKFYVE inhibition leads to ammonium accumulation in vacuoles. Here, impairment of lysosomal function and autophagic flux due to PIKFYVE inhibition was enhanced by glutamine and ammonium. Our results revealed that vacuoles were produced by PIKFYVE inhibition due to the influx of water associated with the accumulation of ammonium ions in the endosomes and lysosomes. This study provides insights into the mechanism of vacuole expansion during PIKFYVE inhibition and suggests an association between PIKFYVE and glutamine–ammonia metabolism.

Results

PIKFYVE inhibition causes endosome and lysosome enlargement

To investigate the effect of PIKFYVE inhibition on cytosolic vacuole formation, DU145 prostate cancer cells were treated with three PIKFYVE inhibitors: YM201636 (YM), apilimod, and SB202190 (SB). Although SB is often used as a p38 mitogen-activated protein kinase (MAPK) inhibitor, it also forms vacuoles via a mechanism other

than p38 MAPK inhibition, which has recently been reported to be due to its inhibitory effect on PIKFYVE [19-21]. Here, treatment with the PIKFYVE inhibitors resulted in the formation of numerous enlarged vacuoles in the cytosol (Figure 1A and B). These vacuoles were observed as spheres that did not stain well with crystal violet, consistent with a previously report [20]. Vacuoles were observed 1 h after YM treatment and gradually expanded over time (Figure 1C; Figure S1). Early endosome marker EEA was partially localized to several relatively small vesicles formed by YM treatment (Figure 1D). In contrast, the localization of lysosomal-associated membrane protein 1 (LAMP1) and RAB7A, markers of late endosomes and lysosomes, was consistent with many enlarged vacuoles. Therefore, most vacuoles formed after PIKFYVE inhibition were derived from the late endosomes and lysosomes. Concanamycin B (ConB) suppresses endosome and lysosome acidification by inhibiting V-ATPase [22]. Chloroquine (CQ), a weak base, also neutralizes the pH by accumulating in lysosomes [23]. Here, treatment with ConB or CQ abolished the YM-induced vacuole enlargement (Figure 1E). This result suggests that the necessity of an acidic environment in the endosome–lysosome for vacuole formation after PIKFYVE inhibition.

Glutamine facilitates PIKFYVE inhibition-induced vacuole enlargement

Vacuolization, which occurs via the expression of a PIKFYVE-binding mutant of *Vac14,* is suppressed by amino acid removal [24]. To investigate the relevance of amino acids in vacuolation induced by PIKFYVE inhibition, cells were treated with PIKFYVE inhibitors in an amino acid-free medium in this study. As shown in Figure 2A, vacuole enlargement by each PIKFYVE inhibitor was suppressed by the amino acid removal. Amino acid depletion leads to the suppression of mechanistic target of rapamycin complex 1 (MTORC1), thus activating autophagy [25]. Inhibition of MTORC1 with rapamycin had no effect on vacuole enlargement following PIKFYVE inhibition (Figure 2B). To determine the specific amino acids critical for vacuole enlargement, we compared the contribution of each amino acid by adding non-essential amino acids (NEAAs) without glutamine, essential amino acids (EAAs), and glutamine to the amino acid-free medium. The presence of glutamine was the most important factor in vacuole enlargement following YM treatment (Figure 2C). Glutamine is mainly catabolized by glutaminase (GLS) in the mitochondria. Mammals contain two GLS genes: the ubiquitously distributed GLS1 and liver-type GLS2. To examine the involvement of GLS in vacuole enlargement, cells were treated with bis-2-(5-phenylacetamido-1,3,4-thiadiazol-2-yl) ethyl sulfide (BPTES) as a GLS1 inhibitor and glutaminase inhibitor 968 (GI968) as a

GLS2 selective inhibitor, as previously described [26]. Both BPTES and GI968 inhibited vacuole enlargement, and further inhibition was observed via co-treatment with both inhibitors (Figure 2D).

Our findings suggest that PIKFYVE inhibition-induced enlargement of vacuoles requires glutamine and its metabolism via GLS.

Ammonia is necessary for PIKFYVE inhibition-induced vacuole enlargement

Glutamine is catabolized into glutamate and ammonia by GLS in mitochondria [27]. Glutamate is then converted to α-ketoglutarate, which enters the tricarboxylic acid (TCA) cycle. Glutamate is also used in the synthesis of glutathione, which contributes to scavenging of reactive oxygen species. To clarify which of these glutamine metabolites are involved in PIKFYVE inhibition-induced vacuole enlargement, metabolite substitutes were added to the glutamine-depleted medium. As shown in Figure 3A and B, the addition of ammonium chloride (NH_4Cl) instead of glutamine was sufficient for vacuole enlargement. In addition, ammonia scavengers 4-phenylbutyric acid (4-PBA) and methyl pyruvate (MP) suppressed vacuole enlargement in the glutamine-containing culture medium (Figure 3C).

Therefore, ammonia derived from glutamine is necessary for vacuole enlargement

induced by PIKFYVE inhibition.

PIKFYVE inhibition leads to ammonium ion accumulation in endosomes and lysosomes

NH_3 can move across lipid membranes via passive diffusion, whereas NH_4^+ requires a transporter to pass through lipid membranes. The mammalian plasma membrane contains the Rhesus (Rh) protein family, which regulates the efflux of intracellularly accumulated NH_4^+ [28]. The pKa of NH_3/NH_4^+ is approximately 9.25. At neutral pH in the cytosol, NH_3 is partially present and can therefore, pass through lipid membranes and enter endosomes and lysosomes. However, in endosomes and lysosomes at pH 4.5–6.5, almost all NH_3 is protonated to NH_4^+ and thus cannot leave the vesicle by passive diffusion. Since the enlargement of vacuoles by PIKFYVE inhibition requires ammonia, it was predicted that the accumulation of NH_4^+ within the endosomes and lysosomes caused their enlargement. Cellular NH_3/NH_4^+ was evaluated using a modified version of Berthelot reaction [29]. Treatment with the PIKFYVE inhibitors led to the accumulation of cellular NH_3/NH_4^+ (Figure 4A). NH_3/NH_4^+ increased over time during YM treatment (Figure 4B). The accumulation of NH_3/NH_4^+ was suppressed by CQ or ConB treatment (Figure 4C). This result suggests that the acidic environment within endosomes and lysosomes induces

the conversion of NH_3 into NH_4^+, resulting in the accumulation of NH_4^+ and enlargement of these vesicles. The accumulation of NH_4^+ is expected to cause water influx owing to the increased osmotic pressure. Vacuole enlargement by YM was inhibited by exposing the cells to hyperosmotic pressure through the addition of sucrose to the medium (Figure 4D). This indicates that the inhibition of PIKFYVE causes NH_4^+ accumulation in endosomes and lysosomes, which leads to water influx and vesicle expansion due to the increase in osmotic pressure.

To confirm that ammonium accumulation occurs in enlarged endosomes and lysosomes, YM-treated cells were exposed to a solution containing graded concentrations of the non-ionic detergent digitonin and the amount of leaked NH_3/NH_4^+ was measured along with the activity of leaked cytosolic lactate dehydrogenase (LDH) and lysosomal cathepsin [30]. LDH leakage due to plasma membrane permeabilization was significantly observed at 10 μg/mL of digitonin, reaching approximately 80% of leakage at the final concentration (200 μg/mL) by 20 μg/mL (Figure 5A). In contrast, cathepsin leakage was not seen until 30 μg/mL and showed a gradual increase from 40 μg/mL. Ammonia leaked gradually from 30 μg/mL digitonin. These results suggest that ammonium accumulates within intracellular organelles, such as endosomes or lysosomes, rather than in the cytoplasm (Figure 5B). Next, we examined whether damage to lysosomal membranes

affected ammonium accumulation. Injury to the lysosomal membrane with L-leucyl-L-leucine methyl ester (LLOMe) in YM-treated cells caused vacuoles to stain with crystal violet (Figure 5C). Ammonium accumulation was markedly reduced in these cells, whereas LDH leakage was negligible under the same treatment (Figure 5D and E). This indicates that LLOMe treatment did not cause critical damage to the cells or leakage of ammonium from the cytoplasm. Ammonium released from the endosomes and lysosomes by LLOMe treatment was possibly reduced in the cells via efflux from the cells or consumption via amino acid metabolism.

Glutamine and ammonium contribute to the decrease in lysosomal function and autophagic flux via PIKFYVE inhibition.

Cathepsins are the most abundant hydrolases, and their dysfunction is associated with various lysosomal storage diseases, such as neuronal ceroid lipofuscinosis 10 [31]. Cathepsins are sorted into endosomes as inactive procathepsins, which are eventually processed into active mature forms consisting of light and heavy chains. Inhibition of PIKFYVE suppresses cathepsin D maturation [11]. Hence, we examined whether glutamine and its metabolite, ammonium, were involved in the maturation of cathepsin D upon PIKFYVE inhibition. As shown in Figure 6A, suppression of cathepsin D

maturation by YM was facilitated by glutamine or ammonium in the medium.

Lysosomes are responsible for autophagic degradation through the formation of autolysosomes via fusion with autophagosomes. The inhibition of PIKFYVE decreases autophagic flux by preventing autolysosomes formation [32]. As DU145 cells lack ATG5, which is required for canonical autophagy, HT29 intestinal epithelial cells were used to evaluate the effect of PIKFYVE inhibition on autophagic flux [33]. Inhibition of PIKFYVE in HT29 cells resulted in glutamine- and ammonium-dependent vacuole enlargement and intracellular accumulation of ammonium, similar to that observed in DU145 cells (Figure S2A–C). YM treatment-induced increase in microtubule-associated protein 1 light chain 3 (LC3)-II levels, indicating autophagosome accumulation, was also enhanced in the presence of glutamine or ammonium in the medium (Figure 6B). Concurrently, accumulation of sequestosome 1 (SQSTM1, also known as p62), a selective substrate for autophagic degradation, was enhanced. These results indicate that glutamine and its metabolite, ammonia, are important for the suppression of autophagic flux by PIKFYVE inhibition.

Involvement of TRPML1 and calcium signaling in PIKFYVE inhibition-induced

vacuole enlargement

PtdIns(3,5)P_2 produced by PIKFYVE, activates mucolipin TRP cation channel 1 (MCOLN1, also known as TRPML1), a cation channel on endosomal and lysosomal membranes [34]. Loss of function of TRPML1 leads to the enlargement of endosomes and lysosomes [35,36]. Here, treatment with MA-SA1, a TRPML1 agonist, suppressed YM-induced vacuole enlargement (Figure 7A). Moreover, ammonium accumulation induced by YM was reduced by mucolipin synthetic agonist 1 (ML-SA1) (Figure 7B). Therefore, suppression of TRPML1 activity by reducing PtdIns(3,5)P_2 production may contribute to ammonium accumulation and endosome and lysosome enlargement during PIKFYVE inhibition.

Finally, the roles of calcium and calmodulin signaling in the changes induced by PIKFYVE inhibition were evaluated. Ca^{2+} and calmodulin are essential for the homotypic and heterotypic fusion of endosomes and lysosomes [37,38]. Application of the Ca^{2+} chelator O,O'-Bis(2-aminophenyl)ethyleneglycol-N,N,N,N'-tetraacetic acid, tetraacetoxymethyl ester (BAPTA-AM) or the calmodulin inhibitor W-13 suppressed YM-induced vacuole enlargement and ammonium accumulation (Figure 7C–F). These results suggest that Ca^{2+} and calmodulin contribute not only to vesicle fusion but also to ammonium accumulation, thereby promoting endosome and lysosome enlargement.

Discussion

In this study, we showed that the enlargement of endosomes and lysosomes by PIKFYVE inhibition was induced by the accumulation of glutamine-derived ammonium. As NH_3 passes through the lipid membrane via passive diffusion, it penetrates the endosomes and lysosomes. However, in a luminal acidic environment, NH_3 is protonated to NH_4^+ and cannot freely pass through the lipid membrane into the cytosol. Here, neutralization of endosomes and lysosomes with CQ or ConB strongly suppressed ammonium accumulation and vacuole enlargement, suggesting that the protonation of NH_3 to NH_4^+ in an acidic environment is crucial for these events.

Efflux of accumulated NH_4^+ in endosomes and lysosomes requires a specific transporter. Recently, solute carrier family 12 member 9 (SLC12A9) was reported as an ammonium-chloride co-transporter that effluxes lysosomal NH_4^+ into the cytoplasm [39]. *SLC12A9* knockout causes osmotic swelling of lysosomes via ammonium accumulation. As SLC12A9 requires luminal Cl^- for ammonium efflux, PIKFYVE may indirectly regulate SLC12A9 by controlling vesicular Cl^- concentrations. Chloride channel (ClC)-7 is a chloride/proton antiporter in endosomes and lysosomes. PtdIns(3,5)P_2 generated by PIKFYVE inhibits ClC-7. Conversely, inhibition of PIKFYVE promotes ClC-7 activity

[40]. Inhibition of PIKFYVE leads to enlargement of endosomes and lysosomes along with luminal hyperacidification and that these changes are exerted by ClC-7 activation [40,41]. In this case, as the luminal concentration of Cl^- should be increased by the activation of ClC-7, the ammonium efflux function of SLC12A9 should not be suppressed by the loss of Cl^-. Thus, it is plausible that PIKFYVE inhibition may affect SLC12A9 function by mechanisms other than regulating luminal Cl^-. In contrast, knockout mice of ClC-7 show vacuolated endosomes and lysosomes [42]. Therefore, it remains possible that a decrease in luminal Cl^- concentration may affect vacuole enlargement and ammonium accumulation. Future studies should assess the effects of PIKFYVE inhibition on Cl^- concentrations in endosomes and lysosomes.

Since accumulation of ammonium in endosomes and lysosomes would be expected to neutralize the luminal pH, the results of previous reports that PIKFYVE inhibition promotes endosomal and lysosomal acidification appear to be contradictory [40,41]. However, once ammonium accumulation reduces the acidity of the vesicles, no further ammonium accumulation or vacuole enlargement is expected to occur, as in the case of V-ATPase inhibition. Our results showed that PIKFYVE inhibition continuously accumulated ammonium over 24 h. Thus, ClC-7-mediated acidification of endosomes and lysosomes may outweigh neutralization by ammonium, leading to persistent ammonium

accumulation.

PtdIns(3,5)P_2 directly activates TRPML1. Vacuole formation in *Vac14* knockout cells is suppressed by TRPML1 overexpression [34]. Additionally, *Trpml1* knockout leads to enlarged vacuoles [35,36]. In this study, we showed that PIKFYVE inhibition-induced vacuole enlargement and ammonium accumulation were reduced by the TRPML1 agonist, ML-SA1. TRPML1 localizes to the endosome–lysosome and contributes to lysosomal homeostasis by controlling vesicular trafficking and lysosomal reformation [43]. Disruption of TRPML1 causes lysosomal acidification and reduction of luminal Cl^- concentration [44,45]. Therefore, TRPML1 and ClC-7 may collaborate to maintain lysosomal function, and inhibition of PIKFYVE may impair the lysosomal system by affecting both channels.

Previously, it was proposed that vacuole expansion due to PIKFYVE inhibition may be due to a shift in the fusion/fission balance of endosomal and lysosomal vesicles toward fusion dominance [18]. Heterotypic and homotypic fusion of endosomes and lysosomes requires Ca^{2+} [37]. The results of this study, in which endosome and lysosome enlargement by PIKFYVE inhibition was suppressed by Ca^{2+} depletion and calmodulin inhibition, are consistent with the previous hypothesis. However, it has also been suggested that this vacuole enlargement is due to osmotic swelling caused by an increase

in luminal solute concentration [41]. Overexpression and activation of the endosomal–lysosomal Ca^{2+} channel P2X4 leads to endosome and lysosome enlargement through the induction of their fusion; however, this enlargement is saturated 1 h after activation [46]. After PIKFYVE inhibition, enlarged vacuoles were also observed within 1 h, and enlargement continued for 24 h. Simultaneously, ammonium accumulation increased by approximately 14-fold after 24 h compared to 1 h. Our results also show that Ca^{2+} and calmodulin are required for ammonium accumulation. These results suggest that Ca^{2+} and calmodulin contribute to vesicle fusion and ammonium accumulation, resulting in am increase in the luminal solute concentration and osmotic swelling of endosomes and lysosomes.

Decreased PtdIns(3,5)P_2 production due to PIKFYVE dysfunction causes various pathological disturbances. Fleck corneal dystrophy (FCD) is an autosomal dominant genetic disease characterized by vacuolar swelling in corneal cells that is caused by *PIKFYVE* [47,48]. Patients with Mucolipidosis type IV, caused by genetic defects in *TRPML1*, a receptor for PtdIns(3,5)P_2, exhibit vacuole accumulation in various organs (Wakabayashi et al., 2011). Here, our results revealed that vacuole enlargements in these diseases may be caused by the accumulation of glutamine-derived ammonium. We also showed that the reduction in lysosomal function and autophagic flux by PIKFYVE

inhibition requires glutamine or ammonium. Therefore, interference with glutamine–ammonia metabolism may alleviate the symptoms associated with these genetic abnormalities. Brain vacuolation is a characteristic feature of prion disease. PIKFYVE is degraded through deacylation in prion disease, resulting in spongiform neurodegeneration [49]. Our results indicate that vacuolation in prion diseases may also be due to the accumulation of ammonium.

PIKFYVE is a potential clinical target for several diseases, including neurodegenerative diseases, such as amyotrophic lateral sclerosis (ALS) and Alzheimer disease, cancer, and viral infections, such as coronavirus disease 2019 (COVID-19) [50]. Most of its action mechanisms are explained by its effects on lysosomal function and autophagy. Our study showed that glutamine and ammonium contribute to a reduction in lysosomal function and autophagic flux upon PIKFYVE inhibition, suggesting that glutamine–ammonia metabolism in therapeutic target cells may influence the effects of these drugs.

This study demonstrated that ammonia derived from glutamine metabolism can be sequestered in intracellular compartments by pharmacological inhibition of PIKFYVE. Excessive ammonia is toxic; therefore, the liver exerts the urea cycle to maintain low serum ammonia concentration. In hepatic encephalopathy, ammonia metabolism

decreases with the liver function, leading to elevated blood ammonia levels and impaired brain function [51]. The effect of ammonia sequestration in endosomes and lysosomes via PIKFYVE inhibition on blood ammonia levels and its impact on the pathology of hyperammonemia warrant future investigation. Increased intracellular ammonia levels promote glutamate synthesis, resulting in the depletion of α-KG, a substrate of the TCA cycle. The resulting decrease in ATP synthesis contributes to the abnormal neurotransmission caused by hyperammonemia [52]. Future studies should investigate whether the sequestration of ammonia in endosomes and lysosomes decreases the cytosolic ammonia levels. A reduction in cytosolic ammonia may also affect amino acid metabolism, such as glutamine synthesis. Cancer cells depend on glutamine and its metabolites for growth [53]. Therefore, the effects of PIKFYVE inhibitors on glutamate–ammonia metabolism may be associated with their efficacy as anticancer drugs.

In conclusion, this study revealed that the enlargement of endosome- and lysosome-derived vacuoles by PIKFYVE inhibition was due to ammonium accumulation. Our results provide important insights into the diseases associated with PIKFYVE dysfunction. Further investigation of the relationship between PIKFYVE and ammonium transporters is necessary to determine cause of ammonium accumulation in endosomes and lysosomes.

Materials and Methods

Materials

All compounds used in this study were from commercial sources. YM201636 (13576), apilimod (19094), SB202190 (21201), BPTES (19284), glutaminase inhibitor compound 968 (17199), rapamycin (13346), and LLOMe (16008) were purchased from Cayman Chemical. Ammonium chloride (015-02991), ML-SA1 (131-18531), MEM NEAA (139-15651), MEM EAA (132-15641), and 200 mM L-glutamine solution (073-05391) were obtained from FUJIFILM Wako Pure Chemical Corporation (Wako). Concanamycin B (BLK-1160) was purchased from BioLinks KK; Dimethyl α-ketoglutarate (K0013), dimethyl L-glutamate hydrochloride (D3353), methyl pyruvate (P0580), digitonin D0540), and W-13 hydrochloride (A2416) were purchased from Tokyo Chemical Industry. Chloroquine diphosphate (08660-04), crystal violet (09804-52), N-acetyl-L-cysteine (00512-84), and 4-(2-Aminoethyl)-benzolsulfonylfluorid-hydrochloride (AEBSF; 02068-64) were obtained from Nacalai Tesque. Sodium 4-phenylbutyrate (4-PBA; P2815) was obtained LKT Laboratories. BAPTA-AM (B035), and 4',6-diamidino-2-phenylindole, dihydrochloride (DAPI; D212) were purchased from Dojindo. benzyloxycarbonyl-L-phenylalanyl-L-arginine 4-methylcoumaryl-7-amide (Z-

FR-MCA; 3095-v) was obtained from the Peptide Institute.

Cell culture and transfection

DU145 and HT29 cells were maintained in RPMI-1640 medium (Nacalai, 30264-56) supplemented with 10% fetal bovine serum and antibiotics (penicillin and streptomycin; Nacalai, 26253-84). The cells were grown in 5% CO_2 at 37°C. DU145 cells were kindly provided by Prof. Toshiyuki Kamoto (Department of Urology, Faculty of Medicine, University of Miyazaki) [54]. HT29 cells were obtained from the American Type Culture Collection (ATCC). Before treatment with PIKFYVE inhibitors (YM, apilimod, and SB), the medium was replaced with the serum-free RPMI-1640 medium. Other compounds (ConB, CQ, rapamycin, BPTES, GI968, 4-PBA, MP, ML-SA1, and W-13) were applied simultaneously with the PIKFYVE inhibitors and incubate for 24 h. The co-treatment time of BAPTA-AM and YM was shortened to avoid cell detachment (6 h in Figure 7C and D). As shown in Figure 5C–E, cells treated with YM for 24 h were challenged with 3 μM LLOMe for 3 h to permeabilize the lysosomal membrane. To estimate the roles of amino acids, the cell culture medium was replaced with the Hank's balanced salt solution (HBSS; Wako, 084-08345) supplemented with 1.5 mM $CaCl_2$, 1.3 mM $MgCl_2$, 19.6 mM $NaHCO_3$, MEM Vitamin Solution (Wako, 130-17141) and antibiotics and mixed with

NEAA, EAA or 2 mM glutamine. As shown in Figure 3A, 2 mM dimethyl α-ketoglutarate, 2 mM dimethyl L-glutamate hydrochloride, 2 mM NH_4Cl or 10 mM NAC was added into HBSS supplemented with NEAA and EAA. Transient transfection was performed using the Xfect Transfection Reagent (Takara Bio, 631316) according to the manufacturer's instructions.

Crystal violet staining

The cells were seeded on coverslips and cultured for 2–3 d. Then, the cells were treated with PIKFYVE inhibitors for 24 h or the indicated time in a serum-free medium and fixed in glyoxal solution with pH adjusted to 4.0 using NaOH [55]. After washing with water, the cells were stained with 0.05% crystal violet solution for 10 min. Coverslips were washed and mounted on glass slides using phosphate-bufferd saline (PBS). Bright-field images were acquired using the BZ-X700 All-in-One inverted fluorescence microscope (Keyence, Osaka, Japan). Area of vacuoles was analyzed with Fiji (Image J) software. Extraction of vacuoles as regions of interest (ROIs) was performed manually after processing using the Trainable Weka Segmentation plug-in [56]. Total area of the vacuoles was normalized to the number of cell nuclei per image. Three images were captured per coverslip, and the average of the analyzed results for each image was

considered as one experiment. Each result was based on at least three independent experiments.

Immunofluorescence assay

DU145 cells grown on coverslips were fixed with 4% paraformaldehyde in PBS for 15 min at room temperature and permeabilized with 0.2% TritonX-100 for 5 min. After permeabilization, the cells were blocked with 0.2% bovine serum albumin and incubated overnight at 4°C with the anti-EEA (1:200; Cell Signaling Technology, 3288) or anti-LAMP1 (1:200; BD Pharmingen, 555798) antibody. The cells were subsequently incubated with the anti-mouse IgG DyLight488 (1:250; Jackson ImmunoResearch, 715-485-151) or anti-rabbit IgG Cy3 (1:250; Jackson ImmunoResearch, 711-165-152) antibody. Subcellular localization of RAB7A was visualized via exogenous expression of mCherry-tagged RAB7A. *RAB7A* was cloned from the cDNA synthesized from total human brain RNA [57] into the pmCherry-N1 plasmid (Clontech Laboratories, 632523). Cells were stained with DAPI, and coverslips were mounted on glass slides using glycerol-DABCO. Images were captured using the LSM710 confocal microscope (Carl Zeiss, Jena, Germany).

Berthelot reaction

Cellular accumulation of ammonia/ammonium was evaluated using a modified version of the Berthelot reaction [29]. Briefly, cells were seeded in 35-mm culture dishes. After PIKFYVE inhibition, cells were detached with 250 μL trypsin solution (Nacalai, 32777-44) and collected in 1.5 mL tubes with 1 mL culture medium. Then, 50 μL of cell suspension was aliquoted for cell counting. Remaining 1200 μL of cell suspension was centrifuged, washed with PBS, centrifuged, and the precipitate was suspended in 100 μL of 80% methanol. After keeping at –30°C for 10 min, the cell suspensions were centrifuged and 15 μL of supernatants were applied to a 96-well dish with 75 μL of solution A (100 mM phenol, 50 mg/L sodium nitroprusside). Next, 75 μL of solution B (0.38 M dibasic sodium phosphate, 125 mM NaOH, and 1% sodium hypochlorite) was added to each well and incubated for 40 min at 37°C. Optical absorbance (Abs) of the aliquots was measured at 635 nm using a microplate reader (TECAN, Infinite M Nano, Männedorf, Switzerland). Abs was subtracted from the background value (80% methanol) and normalized to the number of cells.

Lysosomal membrane permeabilization assay

Accumulation of ammonium in lysosomes was examined based on the difference in

lipid membrane permeability to digitonin between the plasma and lysosomal membranes. The protocol was based on a previously reported method [30]. Briefly, cells seeded on the 24 well dish were treated with YM for 24 h. Then, cells were washed with cold PBS and treated with 200 μL of digitonin extraction buffer (250 mM sucrose, 10 mM KCl, 1.5 mM $MgCl_2$, 1 mM EDTA, 1 mM EGTA, 0.5 mM AEBSF, 20 mM HEPES, pH 7.5) containing the indicated digitonin concentrations. After rocking on ice for 15 min, the supernatants were collected and centrifuged. Ammonium leakage was analyzed using the Berthelot reaction with addition of 75 μL of Solution A and Solution B. LDH leakage was analyzed using the Cytotoxicity LDH Assay Kit-WST (Dojindo, 347-91751), according to the manufacturer's instructions. Cathepsin activity was evaluated based on the kinetics of Z-FR-MCA hydrolysis. The supernatants were mixed with the same volume of cathepsin reaction buffer (50 mM sodium acetate, 4 mM EDTA, 0.5 mM AEBSF, 8 mM dithiothreitol, and 50 μM Z-FR-MCA [pH 6.0]). Fluorescence transition (excitation: 380 nm; emission: 460 nm) was measured at 45 s intervals for 20 min using a fluorescence microplate reader (Fluoroskan Ascent FL, Thermo Labsystems, Waltham, MA, USA).

Western blotting

Samples were prepared and transferred to polyvinylidene difluoride (PVDF)

membranes (Wako, 033-22453) as previously described [58]. The membranes were probed with the appropriate concentrations of primary antibodies against cathepsin D (1:100; Cell Signaling Technology, 2284), glyceraldehyde 3-phosphate dehydrogenase (GAPDH; 1:200; Wako, 016-25523), p62 (1:1000; MBL, M162-3), and LC3B (1:400; MBL, PM036). Immunoreactive proteins were detected using a horseradish-peroxidase-labeled secondary antibody for mouse IgG (1:10,000; Jackson ImmunoResearch, 115-035-003) or for anti-rabbit IgG (1:10,000; Jackson ImmunoResearch, 111-035-003) with EzWestLumi plus (ATTO, WSE-7120S). The signal intensity was calculated using the Fiji software.

Statistical analyses

Data were analyzed using the Prism software (GraphPad Software, San Diego, CA, USA). Data are expressed as mean ± standard deviation. All data were analyzed using the one-way analysis of variance followed by Dunnett's *post-hoc* test, unless stated otherwise in the figure legends. Statistical significance was set at $p < 0.05$.

Acknowledgments

The authors thank Hiroko Matsui for the excellent secretarial assistance. All imaging was performed at the Research Support Center of Medical Research Institute in Kanazawa Medical University.

Disclosure statement

The authors declare that they have no known competing financial interests or personal relationships that could have appeared to influence the work reported in this paper.

Reference

[1] Settembre C, Fraldi A, Medina DL, et al. Signals from the lysosome: a control centre for cellular clearance and energy metabolism. Nat Rev Mol Cell Biol. 2013 May;14(5):283-96. PubMed PMID: 23609508.

[2] La Cognata V, Guarnaccia M, Polizzi A, et al. Highlights on Genomics Applications for Lysosomal Storage Diseases. Cells. 2020 Aug 14;9(8). PubMed PMID: 32824006.

[3] Yang C, Wang X. Lysosome biogenesis: Regulation and functions. J Cell Biol. 2021 Jun 7;220(6). PubMed PMID: 33950241.

[4] Kawai A, Uchiyama H, Takano S, et al. Autophagosome-lysosome fusion depends on the pH in acidic compartments in CHO cells. Autophagy. 2007 Mar-Apr;3(2):154-7. PubMed PMID: 17204842.

[5] Yamamoto A, Tagawa Y, Yoshimori T, et al. Bafilomycin A1 prevents maturation of autophagic vacuoles by inhibiting fusion between autophagosomes and lysosomes in rat hepatoma cell line, H-4-II-E cells. Cell Struct Funct. 1998 Feb;23(1):33-42. PubMed PMID: 9639028.

[6] Takatori S, Tatematsu T, Cheng J, et al. Phosphatidylinositol 3,5-Bisphosphate-Rich Membrane Domains in Endosomes and Lysosomes. Traffic. 2016 Feb;17(2):154-67. PubMed PMID: 26563567.

[7] Hasegawa J, Strunk BS, Weisman LS. PI5P and PI(3,5)P(2): Minor, but Essential Phosphoinositides. Cell Struct Funct. 2017 May 3;42(1):49-60. PubMed PMID: 28302928.

[8] Zolov SN, Bridges D, Zhang Y, et al. In vivo, Pikfyve generates PI(3,5)P2, which serves as both a signaling lipid and the major precursor for PI5P. Proc Natl Acad Sci U S A. 2012 Oct 23;109(43):17472-7. PubMed PMID: 23047693.

[9] Bissig C, Hurbain I, Raposo G, et al. PIKfyve activity regulates reformation of terminal storage lysosomes from endolysosomes. Traffic. 2017 Nov;18(11):747-757. PubMed PMID: 28857423.

[10] Yordanov TE, Hipolito VEB, Liebscher G, et al. Biogenesis of lysosome-related organelles complex-1 (BORC) regulates late endosomal/lysosomal size through PIKfyve-dependent phosphatidylinositol-3,5-bisphosphate. Traffic. 2019 Sep;20(9):674-696. PubMed PMID: 31314175.

[11] Sano O, Kazetani K, Funata M, et al. Vacuolin-1 inhibits autophagy by impairing lysosomal maturation via PIKfyve inhibition. FEBS Lett. 2016 Jun;590(11):1576-85. PubMed PMID: 27135648.

[12] Sharma G, Guardia CM, Roy A, et al. A family of PIKFYVE inhibitors with therapeutic potential against autophagy-dependent cancer cells disrupt multiple events in lysosome homeostasis. Autophagy. 2019 Oct;15(10):1694-1718. PubMed PMID: 30806145.

[13] Ikonomov OC, Sbrissa D, Delvecchio K, et al. The phosphoinositide kinase PIKfyve is vital in early embryonic development: preimplantation lethality of PIKfyve-/- embryos but normality of PIKfyve+/- mice. J Biol Chem. 2011 Apr 15;286(15):13404-13. PubMed PMID: 21349843.

[14] Takasuga S, Horie Y, Sasaki J, et al. Critical roles of type III phosphatidylinositol phosphate kinase in murine embryonic visceral endoderm and adult intestine. Proc Natl Acad Sci U S A. 2013 Jan 29;110(5):1726-31. PubMed PMID: 23322734.

[15] Chow CY, Zhang Y, Dowling JJ, et al. Mutation of FIG4 causes neurodegeneration in the pale tremor mouse and patients with CMT4J. Nature. 2007 Jul 5;448(7149):68-72. PubMed PMID: 17572665.

[16] Zhang Y, Zolov SN, Chow CY, et al. Loss of Vac14, a regulator of the signaling lipid phosphatidylinositol 3,5-bisphosphate, results in neurodegeneration in mice. Proc Natl Acad Sci U S A. 2007 Oct 30;104(44):17518-23. PubMed PMID: 17956977.

[17] Ikonomov OC, Sbrissa D, Mlak K, et al. Functional dissection of lipid and protein kinase signals of PIKfyve reveals the role of PtdIns 3,5-P2 production for endomembrane integrity. J Biol Chem. 2002 Mar 15;277(11):9206-11. PubMed PMID: 11714711.

[18] Choy CH, Saffi G, Gray MA, et al. Lysosome enlargement during inhibition of the lipid kinase PIKfyve proceeds through lysosome coalescence. J Cell Sci. 2018 May 21;131(10). PubMed PMID: 29661845.

[19] Wible DJ, Parikh Z, Cho EJ, et al. Unexpected inhibition of the lipid kinase

PIKfyve reveals an epistatic role for p38 MAPKs in endolysosomal fission and volume control. Cell Death Dis. 2024 Jan 22;15(1):80. PubMed PMID: 38253602.

[20] Menon MB, Kotlyarov A, Gaestel M. SB202190-induced cell type-specific vacuole formation and defective autophagy do not depend on p38 MAP kinase inhibition. PLoS One. 2011;6(8):e23054. PubMed PMID: 21853067.

[21] Menon MB, Dhamija S, Kotlyarov A, et al. The problem of pyridinyl imidazole class inhibitors of MAPK14/p38alpha and MAPK11/p38beta in autophagy research. Autophagy. 2015;11(8):1425-7. PubMed PMID: 26061537.

[22] Woo JT, Shinohara C, Sakai K, et al. Inhibition of the acidification of endosomes and lysosomes by the antibiotic concanamycin B in macrophage J774. Eur J Biochem. 1992 Jul 1;207(1):383-9. PubMed PMID: 1628660.

[23] Poole B, Ohkuma S. Effect of weak bases on the intralysosomal pH in mouse peritoneal macrophages. J Cell Biol. 1981 Sep;90(3):665-9. PubMed PMID: 6169733.

[24] Schulze U, Vollenbroker B, Kuhnl A, et al. Cellular vacuolization caused by overexpression of the PIKfyve-binding deficient Vac14(L156R) is rescued by starvation and inhibition of vacuolar-ATPase. Biochim Biophys Acta Mol Cell Res. 2017 May;1864(5):749-759. PubMed PMID: 28216340.

[25] Takahara T, Amemiya Y, Sugiyama R, et al. Amino acid-dependent control of mTORC1 signaling: a variety of regulatory modes. J Biomed Sci. 2020 Aug 17;27(1):87. PubMed PMID: 32799865.

[26] Lukey MJ, Cluntun AA, Katt WP, et al. Liver-Type Glutaminase GLS2 Is a Druggable Metabolic Node in Luminal-Subtype Breast Cancer. Cell Rep. 2019 Oct 1;29(1):76-88 e7. PubMed PMID: 31577957.

[27] Altman BJ, Stine ZE, Dang CV. From Krebs to clinic: glutamine metabolism to cancer therapy. Nat Rev Cancer. 2016 Oct;16(10):619-34. PubMed PMID: 27492215.

[28] Williamson G, Harris T, Bizior A, et al. Biological ammonium transporters: evolution and diversification. FEBS J. 2024 Jan 24. PubMed PMID: 38265636.

[29] Spinelli JB, Kelley LP, Haigis MC. An LC-MS Approach to Quantitative Measurement of Ammonia Isotopologues. Sci Rep. 2017 Sep 4;7(1):10304. PubMed PMID: 28871132.

[30] Jaattela M, Nylandsted J. Quantification of Lysosomal Membrane Permeabilization by Cytosolic Cathepsin and beta-N-Acetyl-Glucosaminidase Activity Measurements. Cold Spring Harb Protoc. 2015 Nov 2;2015(11):1017-23. PubMed PMID: 26527764.

[31] Drobny A, Prieto Huarcaya S, Dobert J, et al. The role of lysosomal cathepsins in neurodegeneration: Mechanistic insights, diagnostic potential and therapeutic approaches. Biochim Biophys Acta Mol Cell Res. 2022 Jul;1869(7):119243. PubMed PMID: 35217144.

[32] Martin S, Harper CB, May LM, et al. Inhibition of PIKfyve by YM-201636 dysregulates autophagy and leads to apoptosis-independent neuronal cell death. PLoS One. 2013;8(3):e60152. PubMed PMID: 23544129.

[33] Peng K, Sun A, Zhu J, et al. Restoration of the ATG5-dependent autophagy sensitizes DU145 prostate cancer cells to chemotherapeutic drugs. Oncol Lett. 2021 Sep;22(3):638. PubMed PMID: 34386060.

[34] Dong XP, Shen D, Wang X, et al. PI(3,5)P(2) controls membrane trafficking by direct activation of mucolipin Ca(2+) release channels in the endolysosome. Nat Commun. 2010 Jul 13;1(4):38. PubMed PMID: 20802798.

[35] Remis NN, Wiwatpanit T, Castiglioni AJ, et al. Mucolipin co-deficiency causes accelerated endolysosomal vacuolation of enterocytes and failure-to-thrive from birth to weaning. PLoS Genet. 2014 Dec;10(12):e1004833. PubMed PMID: 25521295.

[36] Venugopal B, Browning MF, Curcio-Morelli C, et al. Neurologic, gastric, and

opthalmologic pathologies in a murine model of mucolipidosis type IV. Am J Hum Genet. 2007 Nov;81(5):1070-83. PubMed PMID: 17924347.

[37] Pryor PR, Mullock BM, Bright NA, et al. The role of intraorganellar Ca(2+) in late endosome-lysosome heterotypic fusion and in the reformation of lysosomes from hybrid organelles. J Cell Biol. 2000 May 29;149(5):1053-62. PubMed PMID: 10831609.

[38] Colombo MI, Beron W, Stahl PD. Calmodulin regulates endosome fusion. J Biol Chem. 1997 Mar 21;272(12):7707-12. PubMed PMID: 9065429.

[39] Levin-Konigsberg R, Mitra K, Nigam A, et al. SLC12A9 is a lysosome-detoxifying ammonium - chloride co-transporter. bioRxiv. 2023 May 22. PubMed PMID: 37292735.

[40] Leray X, Hilton JK, Nwangwu K, et al. Tonic inhibition of the chloride/proton antiporter ClC-7 by PI(3,5)P2 is crucial for lysosomal pH maintenance. Elife. 2022 Jun 7;11. PubMed PMID: 35670560.

[41] Cao X, Lenk GM, Mikusevic V, et al. The chloride antiporter CLCN7 is a modifier of lysosome dysfunction in FIG4 and VAC14 mutants. PLoS Genet. 2023 Jun;19(6):e1010800. PubMed PMID: 37363915.

[42] Wartosch L, Fuhrmann JC, Schweizer M, et al. Lysosomal degradation of

endocytosed proteins depends on the chloride transport protein ClC-7. FASEB J. 2009 Dec;23(12):4056-68. PubMed PMID: 19661288.

[43] Venkatachalam K, Wong CO, Zhu MX. The role of TRPMLs in endolysosomal trafficking and function. Cell Calcium. 2015 Jul;58(1):48-56. PubMed PMID: 25465891.

[44] Miedel MT, Rbaibi Y, Guerriero CJ, et al. Membrane traffic and turnover in TRP-ML1-deficient cells: a revised model for mucolipidosis type IV pathogenesis. J Exp Med. 2008 Jun 9;205(6):1477-90. PubMed PMID: 18504305.

[45] Lee D, Hong JH. Modulation of Lysosomal Cl(-) Mediates Migration and Apoptosis through the TRPML1 as a Lysosomal Cl(-) Sensor. Cells. 2023 Jul 12;12(14). PubMed PMID: 37508500.

[46] Cao Q, Zhong XZ, Zou Y, et al. Calcium release through P2X4 activates calmodulin to promote endolysosomal membrane fusion. J Cell Biol. 2015 Jun 22;209(6):879-94. PubMed PMID: 26101220.

[47] Li S, Tiab L, Jiao X, et al. Mutations in PIP5K3 are associated with Francois-Neetens mouchetee fleck corneal dystrophy. Am J Hum Genet. 2005 Jul;77(1):54-63. PubMed PMID: 15902656.

[48] Kawasaki S, Yamasaki K, Nakagawa H, et al. A novel mutation

(p.Glu1389AspfsX16) of the phosphoinositide kinase, FYVE finger containing gene found in a Japanese patient with fleck corneal dystrophy. Mol Vis. 2012;18:2954-60. PubMed PMID: 23288988.

[49] Lakkaraju AKK, Frontzek K, Lemes E, et al. Loss of PIKfyve drives the spongiform degeneration in prion diseases. EMBO Mol Med. 2021 Sep 7;13(9):e14714. PubMed PMID: 34291577.

[50] Burke JE, Triscott J, Emerling BM, et al. Beyond PI3Ks: targeting phosphoinositide kinases in disease. Nat Rev Drug Discov. 2023 May;22(5):357-386. PubMed PMID: 36376561.

[51] Braissant O, McLin VA, Cudalbu C. Ammonia toxicity to the brain. J Inherit Metab Dis. 2013 Jul;36(4):595-612. PubMed PMID: 23109059.

[52] Drews L, Zimmermann M, Westhoff P, et al. Ammonia inhibits energy metabolism in astrocytes in a rapid and glutamate dehydrogenase 2-dependent manner. Dis Model Mech. 2020 Nov 4;13(10). PubMed PMID: 32917661.

[53] Jin J, Byun JK, Choi YK, et al. Targeting glutamine metabolism as a therapeutic strategy for cancer. Exp Mol Med. 2023 Apr;55(4):706-715. PubMed PMID: 37009798.

[54] Kamibeppu T, Yamasaki K, Nakahara K, et al. Caveolin-1 and -2 regulate cell

motility in castration-resistant prostate cancer. Res Rep Urol. 2018;10:135-144. PubMed PMID: 30324095.

[55] Richter KN, Revelo NH, Seitz KJ, et al. Glyoxal as an alternative fixative to formaldehyde in immunostaining and super-resolution microscopy. EMBO J. 2018 Jan 4;37(1):139-159. PubMed PMID: 29146773.

[56] Arganda-Carreras I, Kaynig V, Rueden C, et al. Trainable Weka Segmentation: a machine learning tool for microscopy pixel classification. Bioinformatics. 2017 Aug 1;33(15):2424-2426. PubMed PMID: 28369169.

[57] Khan MR, Uwada J, Yazawa T, et al. Activation of muscarinic cholinoceptor ameliorates tumor necrosis factor-alpha-induced barrier dysfunction in intestinal epithelial cells. FEBS Lett. 2015 Nov 30;589(23):3640-7. PubMed PMID: 26519558.

[58] Uwada J, Mukai S, Terada N, et al. Pleiotropic effects of probenecid on three-dimensional cultures of prostate cancer cells. Life Sci. 2021 Aug 1;278:119554. PubMed PMID: 33932444.

Figure Legends

Figure 1. Inhibition of PIKFYVE causes enlarged endosomes and lysosomes. (**A and B**) DU145 cells were treated with 1 μM YM201636 (YM), 0.03 μM apilimod, 20 μM SB202190 (SB) or dimethyl sulfoxide (DMSO; final: 0.5%) for 24 h. (**A**) Representative images of crystal violet-stained cells. Bar = 20 μm. (**B**) Area of vacuoles per nuclei. ***$p < 0.001$ (compared to DMSO; n = 3). (**C**) Time-course of vacuole enlargement after 1 μM YM treatment (n = 3). (**D**) DU145 cells were treated with 1 μM YM or DMSO (final: 0.5%). Immunofluorescence images for EEA or LAMP1, or mCherry-RAB7A (left panels) and bright-field images of cells (middle panels) were merged with DAPI staining (right panels). Bar = 10 μm (**E**) DU145 cells were co-treated with 1 μM YM and 50 μM chloroquine (CQ) or 0.1 μM concanamycin B (ConB) for 24 h. After crystal violet staining, area of vacuoles was quantified (n = 3).

Figure 2. Glutamine facilitates PIKFYVE inhibition-induced vacuole enlargement. (**A**) DU145 cells were treated with 1 μM YM, 0.03 μM apilimod, and 20 μM SB in RPMI-1640 (RPMI) or amino acid-free HBSS medium. Representative images of crystal violet-stained cells. Bar = 20 μm. (**B**) DU145 cells were co-treated with 1 μM YM and 0.1 μM rapamycin for 24 h. After crystal violet staining, area of vacuoles was quantified (n = 3).

NS, not significantly different via Student's *t*-test. (**C**) DU145 cells were treated with 1 μM YM in HBSS medium with NEAAs, EAAs or glutamine (Gln). After crystal violet staining, area of vacuoles was quantified. NS, not significantly different. **$p < 0.01$ and ***$p < 0.001$ (compared to YM without amino acids; n = 3). (**D**) DU145 cells were co-treated with 1 μM YM and 10 μM BPTES or 20 μM GI968 for 24 h. After crystal violet staining, area of vacuoles was quantified (n = 3). ***$p < 0.001$ (compared to YM).

Figure 3. Ammonia is necessary for PIKFYVE inhibition-induced vacuole enlargement. (**A and B**) DU145 cells were treated with 1 μM YM in HBSS supplemented with 2 mM ammonium chloride (NH_4Cl), 2 mM dimethyl-2-ketoglutarate (cell-permeable α-ketoglutarate [α-Keto]), 2 mM dimethyl glutamate (cell-permeable glutamate [Glu]) and 10 mM N-acetyl-L-cysteine (NAC) for 24 h. (**A**) Representative images of crystal violet-stained cells. Bar = 20 μm. (**B**) Area of vacuoles per nuclei. NS, not significantly different. ***$p < 0.001$ (compared to YM; n = 3). (**C**) DU145 cells were co-treated with 1 μM YM and 5 mM 4-PBA or 20 mM methyl pyruvate (MP) for 24 h. After crystal violet staining, area of vacuoles was quantified (n = 3). ***$p < 0.001$ (compared to YM).

Figure 4. PIKFYVE inhibition leads to ammonium ion accumulation. (**A**) DU145 cells

were treated with 1 μM YM, 0.03 μM apilimod, 20 μM SB or DMSO (final: 0.5%) for 24 h. Each cellular NH_3/NH_4^+ was evaluated using the Berthelot reaction (n = 5). *p < 0.05, ***p < 0.001 (compared to DMSO). (**B**) Time-course of cellular NH_3/NH_4^+ accumulation after 1 μM YM or DMSO (final: 0.5%) treatment (n = 3–6). (**C**) DU145 cells were co-treated with 1 μM YM and 50 μM CQ or 0.1 μM ConB for 24 h. Each cellular NH_3/NH_4^+ was evaluated using the Berthelot reaction (n = 3). (**D**) DU145 cells were challenged with osmotic stress by the addition of 200 mM sucrose simultaneously with 1 μM YM (pre) or after 24 h YM treatment for 6 h (post). After crystal violet staining, area of vacuoles was quantified (n = 3). *p < 0.05 and ***p < 0.001 (compared to YM).

Figure 5. Ammonium accumulation occurs in endosomes and lysosomes during PIKFYVE inhibition. (**A**) Lysosomal permeabilization experiment of DU145 cells. After treating with 1 μM YM for 24 h, DU145 cells were treated with the indicated concentration of digitonin buffer. Leaked NH_3/NH_4^+, LDH, and cathepsin from cells were analyzed (n = 5–6). *p < 0.05, **p < 0.01 and ***p < 0.001 (compared to 0 μg/mL digitonin). (**B**) Schematic diagram of the lysosomal permeabilization experiment. Dashed lines represent the lipid membranes with holes in response to increasing digitonin concentrations. CP = cathepsin. (**C**–**E**) After 24 h of treatment with 1 μM YM, 3 mM

LLOMe was applied to the cells. (**C**) Representative images of crystal violet-stained cells. White arrows indicate the vacuoles that became stained with crystal violet after LLOMe treatment. Bar = 20 μm. (**D**) Reduction of cellular NH_3/NH_4^+ accumulation by LLOMe treatment for 3 h (n = 3). ***$p < 0.001$ (Student's *t*-test). (**E**) Leaked cytosolic LDH after sequential treatment with 3 mM LLOMe for 3 h and 200 μg/mL digitonin for 15 min (n = 4).

Figure 6. Glutamine and ammonia contribute to the decrease in lysosomal function and autophagic flux via PIKFYVE inhibition. (**A**) DU145 cells were treated with 1 μM YM for 24 h in HBSS medium containing 2 mM Gln or 2 mM NH_4Cl. Cell lysates were analyzed via immunoblotting using cathepsin D and GAPDH antibodies. As indicated by the arrows, procathepsin D was observed at high molecular weights, whereas the heavy chain of mature cathepsin D was observed at low molecular weights. The reduced level of mature cathepsin D was quantified as the ratio of procathepsin D to cathepsin D heavy chain (right side). **$p < 0.01$ (n = 6). (**B**) HT29 cells were treated with 0.3 μM YM for 24 h in HBSS medium containing 2 mM Gln or 2 mM NH_4Cl. Cell lysates were analyzed via immunoblotting using p62, LC-3 and GAPDH antibodies. The decrease in autophagic flux was estimated by the increase in the standard autophagy marker, LC3-II, relative to

LC3-I and the accumulation of autophagy substrate p62 (right side). *$p < 0.05$, **$p < 0.01$, and ***$p < 0.001$ ($n = 4$).

Figure 7. Involvement of TRPML1 and calcium signaling in PIKFYVE inhibition-induced vacuole enlargement. (**A and B**) DU145 cells were co-treated with 1 μM YM and 20 μM ML-SA1 or DMSO (final: 0.5%) for 24 h. (**A**) After crystal violet staining, area of vacuoles was quantified. (**B**) Each cellular NH_3/NH_4^+ was evaluated using the Berthelot reaction. ***$p < 0.001$ ($n = 3$). (**C and D**) DU145 cells were co-treated with 1 μM YM and 20 μM BAPTA-AM or DMSO (final 0.5%) for 6 h. (**C**) After crystal violet staining, area of vacuoles was quantified. (**D**) Each cellular NH_3/NH_4^+ was evaluated using the Berthelot reaction. *$p < 0.05$ and ***$p < 0.001$ (Student's *t*-test; $n = 3$). (**E and F**) DU145 cells were co-treated with 1 μM YM and 20 μM W-13 or DMSO (final: 0.5%) for 24 h. (**E**) After crystal violet staining, area of vacuoles was quantified. (**F**) Each cellular NH_3/NH_4^+ was evaluated using the Berthelot reaction. ***$p < 0.001$ (Student's *t*-test; $n = 3$).

Fig. 1

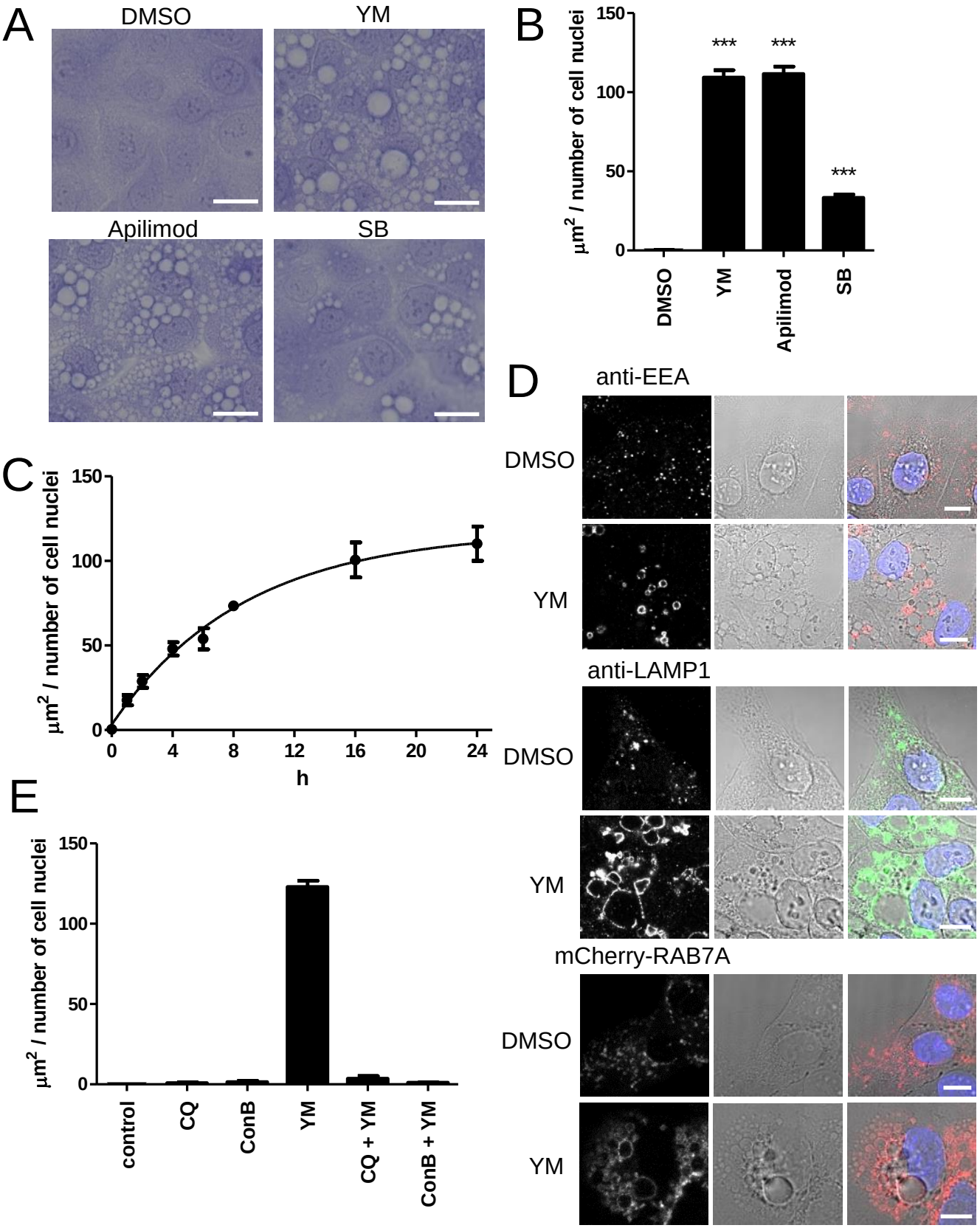
A
DMSO
YM
Apilimod
SB
B
µm² / number of cell nuclei
150
100
50
0
***
***
***
DMSO
YM
Apilimod
SB
C
µm² / number of cell nuclei
150
100
50
0
0
4
8
12
16
20
24
h
D
anti-EEA
DMSO
YM
anti-LAMP1
DMSO
YM
mCherry-RAB7A
DMSO
YM
E
µm² / number of cell nuclei
150
100
50
0
control
CQ
ConB
YM
CQ + YM
ConB + YM

Fig. 2

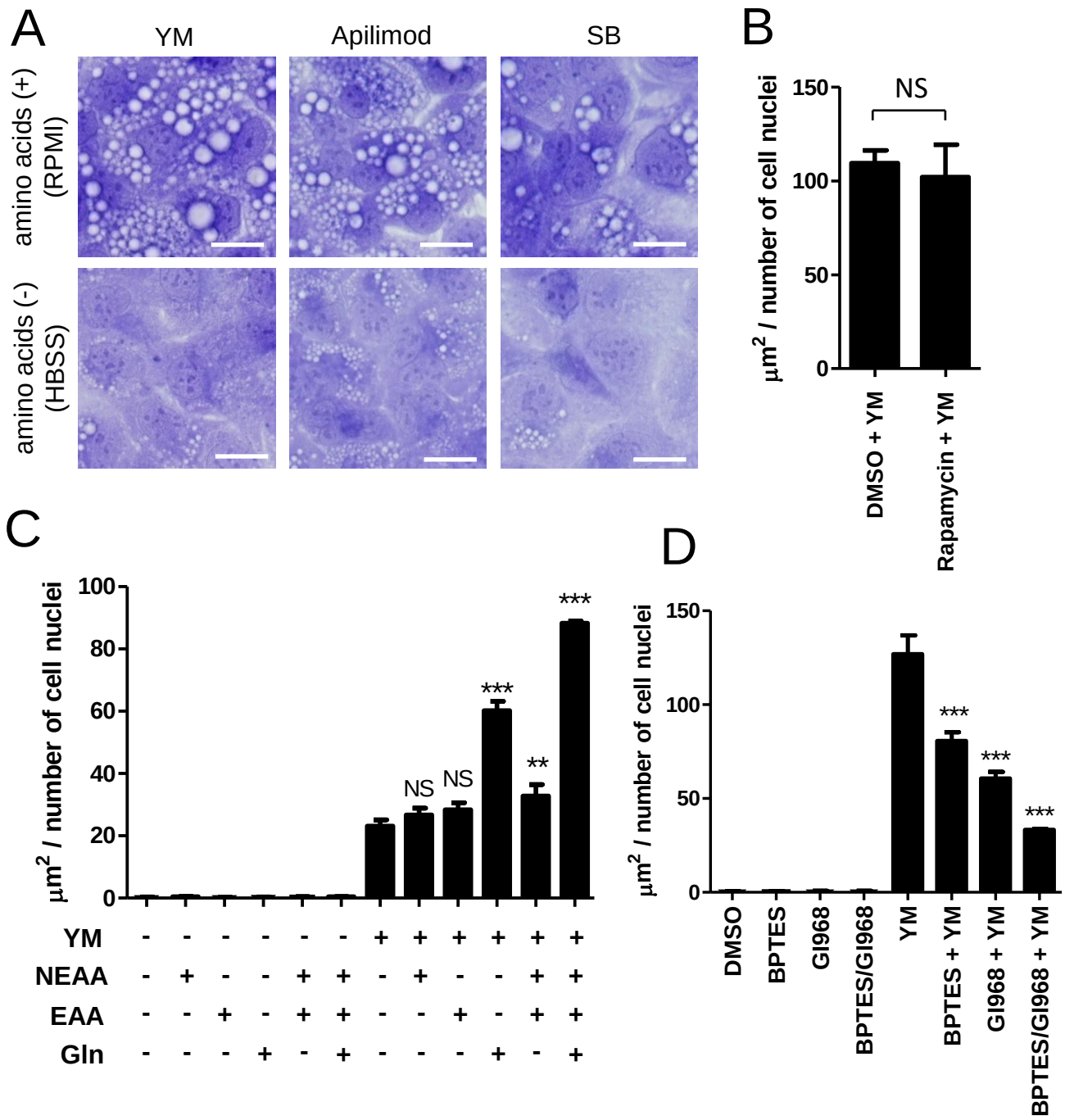
A
YM
Apilimod
SB
amino acids (+) (RPMI)
amino acids (-) (HBSS)
B
NS
150
100
50
0
μm2 / number of cell nuclei
DMSO + YM
Rapamycin + YM
C
100
80
60
40
20
0
μm2 / number of cell nuclei
NS
NS
***
**
***
YM - - - - - - + + + + + +
NEAA - + - - + + - + - - + +
EAA - - + - + + - - + - + +
Gln - - - + - + - - - + - +
D
150
100
50
0
μm2 / number of cell nuclei
***
***
***
DMSO
BPTES
GI968
BPTES/GI968
YM
BPTES + YM
GI968 + YM
BPTES/GI968 + YM

Fig. 3

A

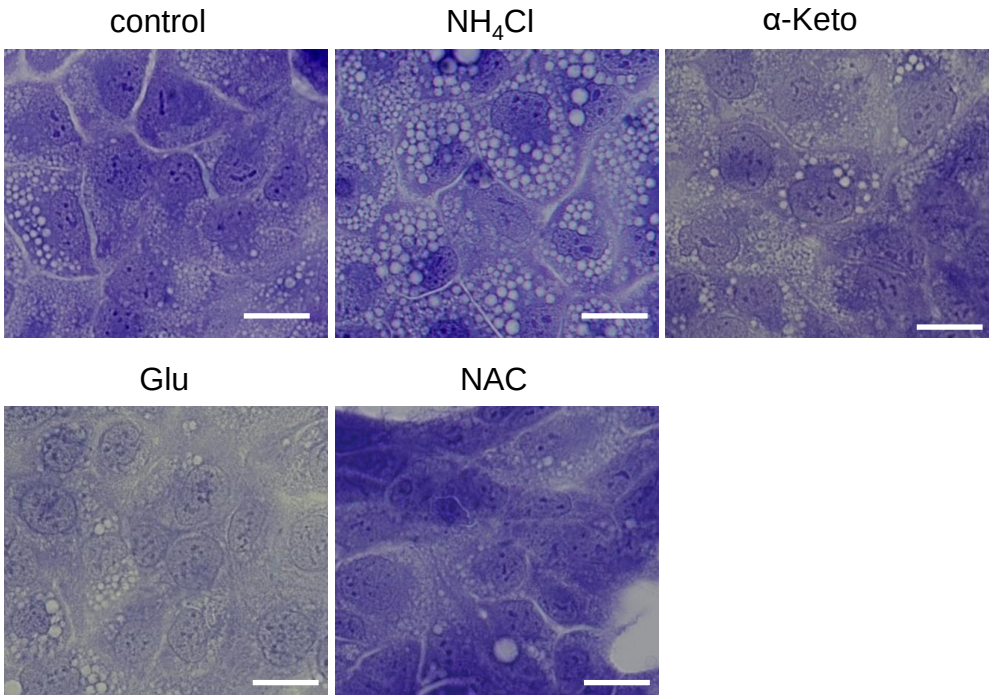
control
NH4Cl
α-Keto
Glu
NAC

B

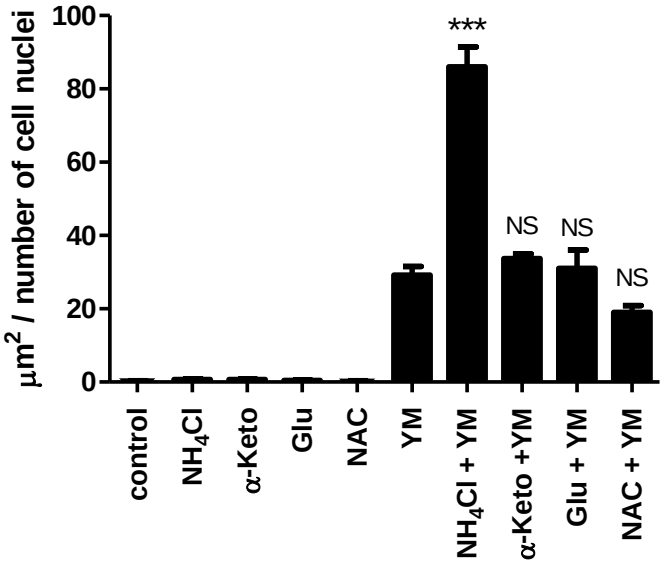
μm2 / number of cell nuclei
100
80
60
40
20
0
***
NS
NS
NS
control
NH4Cl
α-Keto
Glu
NAC
YM
NH4Cl + YM
α-Keto +YM
Glu + YM
NAC + YM

C

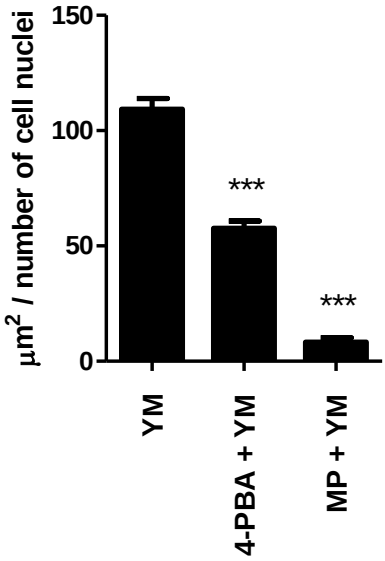
μm2 / number of cell nuclei
150
100
50
0
***
***
YM
4-PBA + YM
MP + YM

Fig. 4

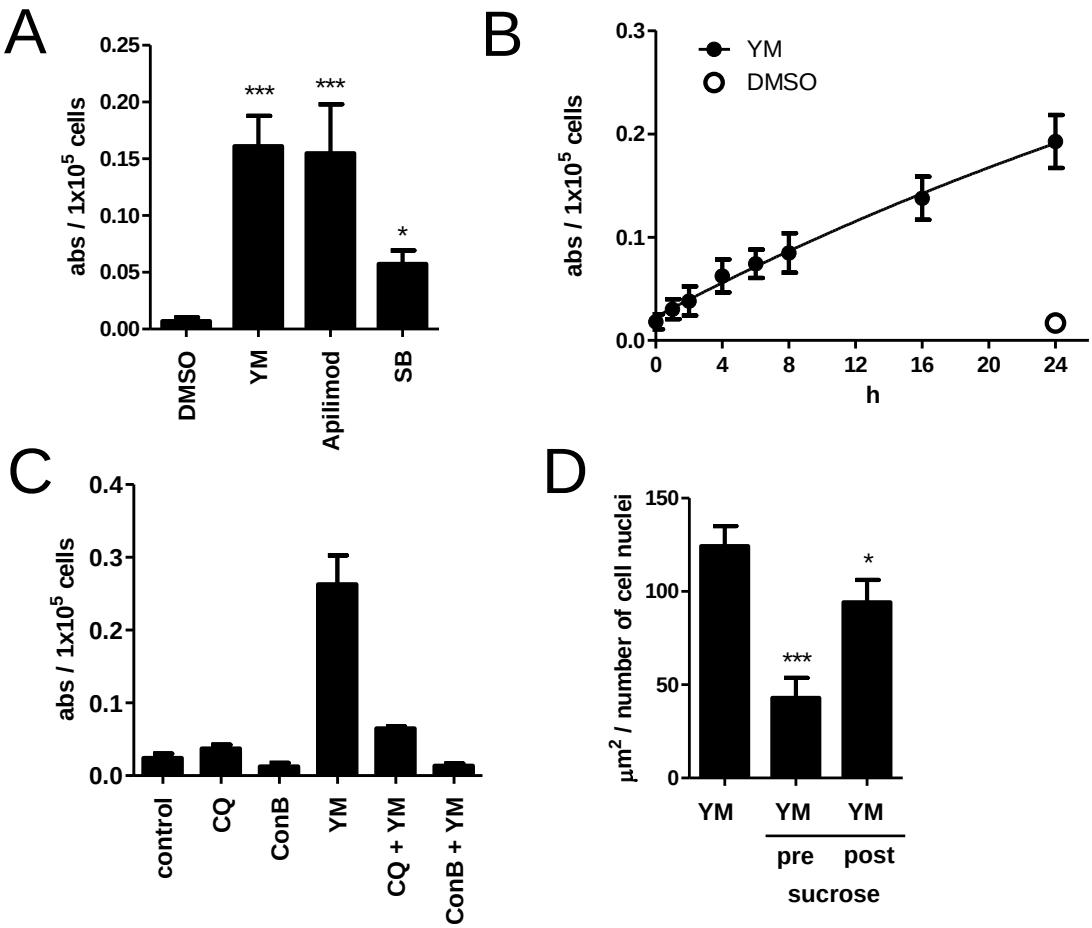
A
abs / 1x10^5 cells
0.25
0.20
0.15
0.10
0.05
0.00
***
***
*
DMSO
YM
Apilimod
SB
B
YM
DMSO
abs / 1x10^5 cells
0.3
0.2
0.1
0.0
0
4
8
12
16
20
24
h
C
abs / 1x10^5 cells
0.4
0.3
0.2
0.1
0.0
control
CQ
ConB
YM
CQ + YM
ConB + YM
D
µm^2 / number of cell nuclei
150
100
50
0
***
*
YM
YM
YM
pre
post
sucrose

Fig. 5

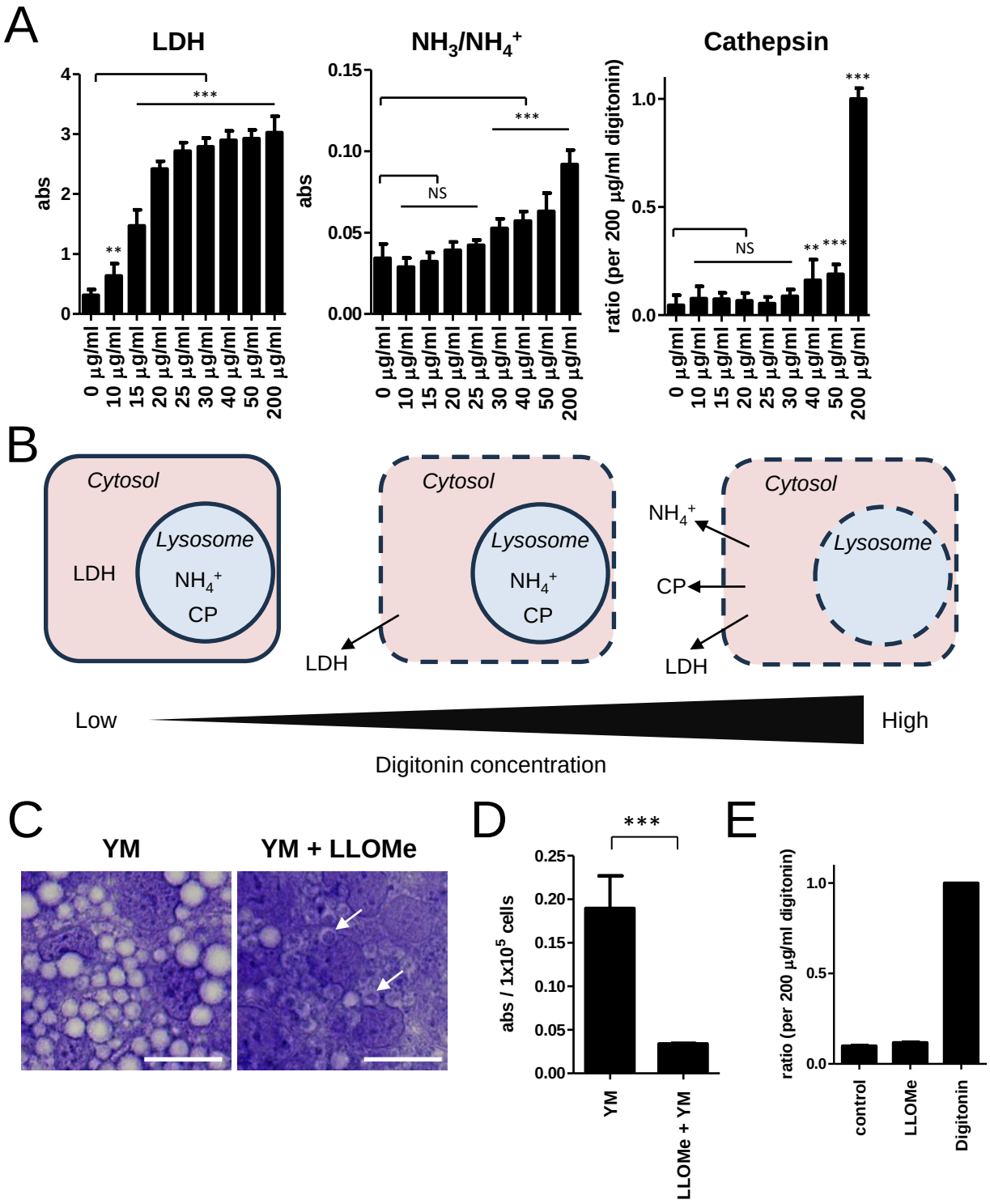
A
LDH
NH3/NH4+
Cathepsin
abs
ratio (per 200 µg/ml digitonin)
0 µg/ml
10 µg/ml
15 µg/ml
20 µg/ml
25 µg/ml
30 µg/ml
40 µg/ml
50 µg/ml
200 µg/ml
NS
B
Cytosol
Lysosome
LDH
NH4+
CP
Low
High
Digitonin concentration
C
YM
YM + LLOMe
D
abs / 1x10^5 cells
YM
LLOMe + YM
E
control
LLOMe
Digitonin

Fig. 6

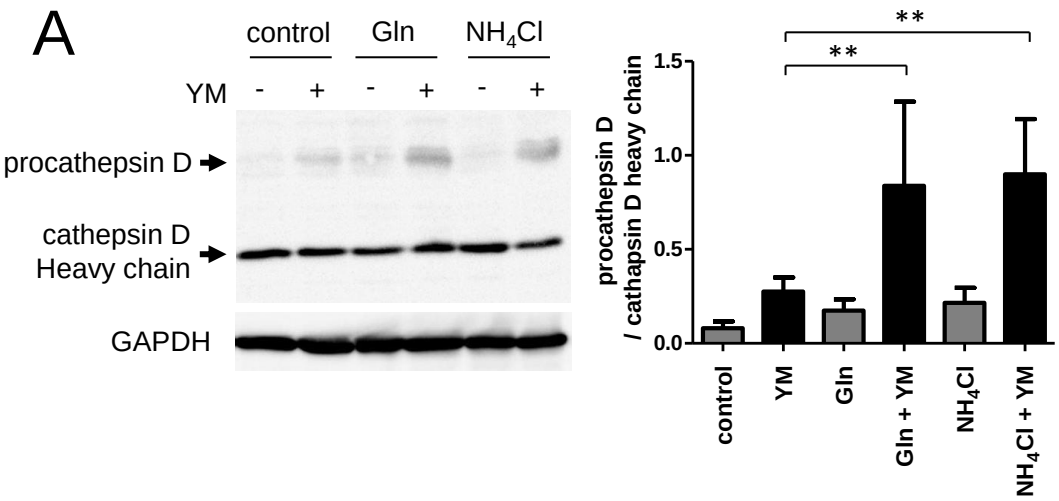
A
control
Gln
NH4Cl
YM
- + - + - +
procathepsin D
cathepsin D
Heavy chain
GAPDH
procathepsin D
/ cathapsin D heavy chain
1.5
1.0
0.5
0.0
**
**
control
YM
Gln
Gln + YM
NH4Cl
NH4Cl + YM

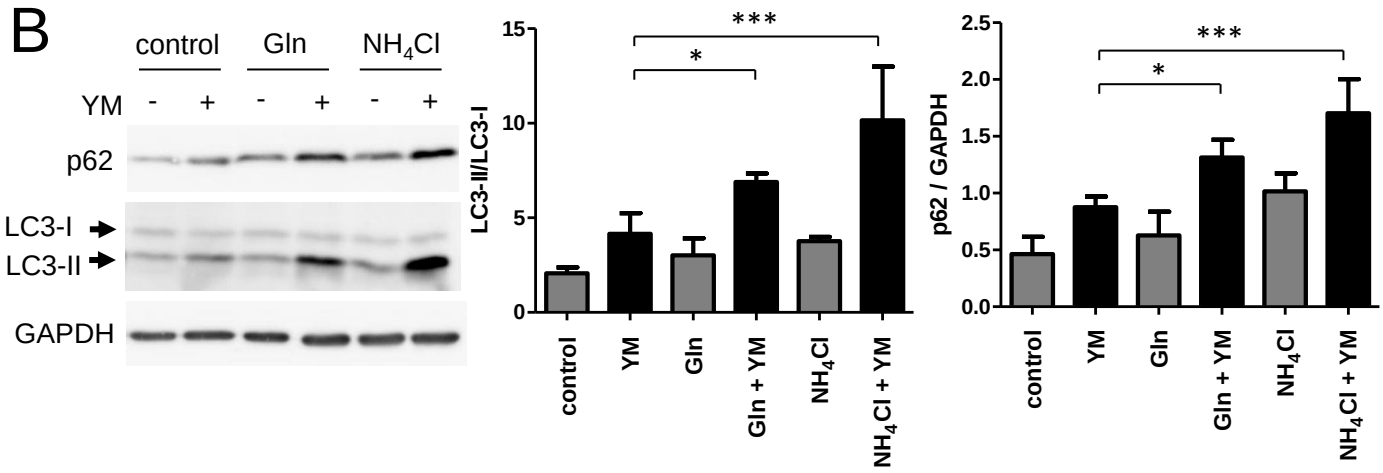
B
control
Gln
NH4Cl
YM
- + - + - +
p62
LC3-I
LC3-II
GAPDH
LC3-II/LC3-I
15
10
5
0
***
*
p62 / GAPDH
2.5
2.0
1.5
1.0
0.5
0.0
***
*
control
YM
Gln
Gln + YM
NH4Cl
NH4Cl + YM

Fig. 7

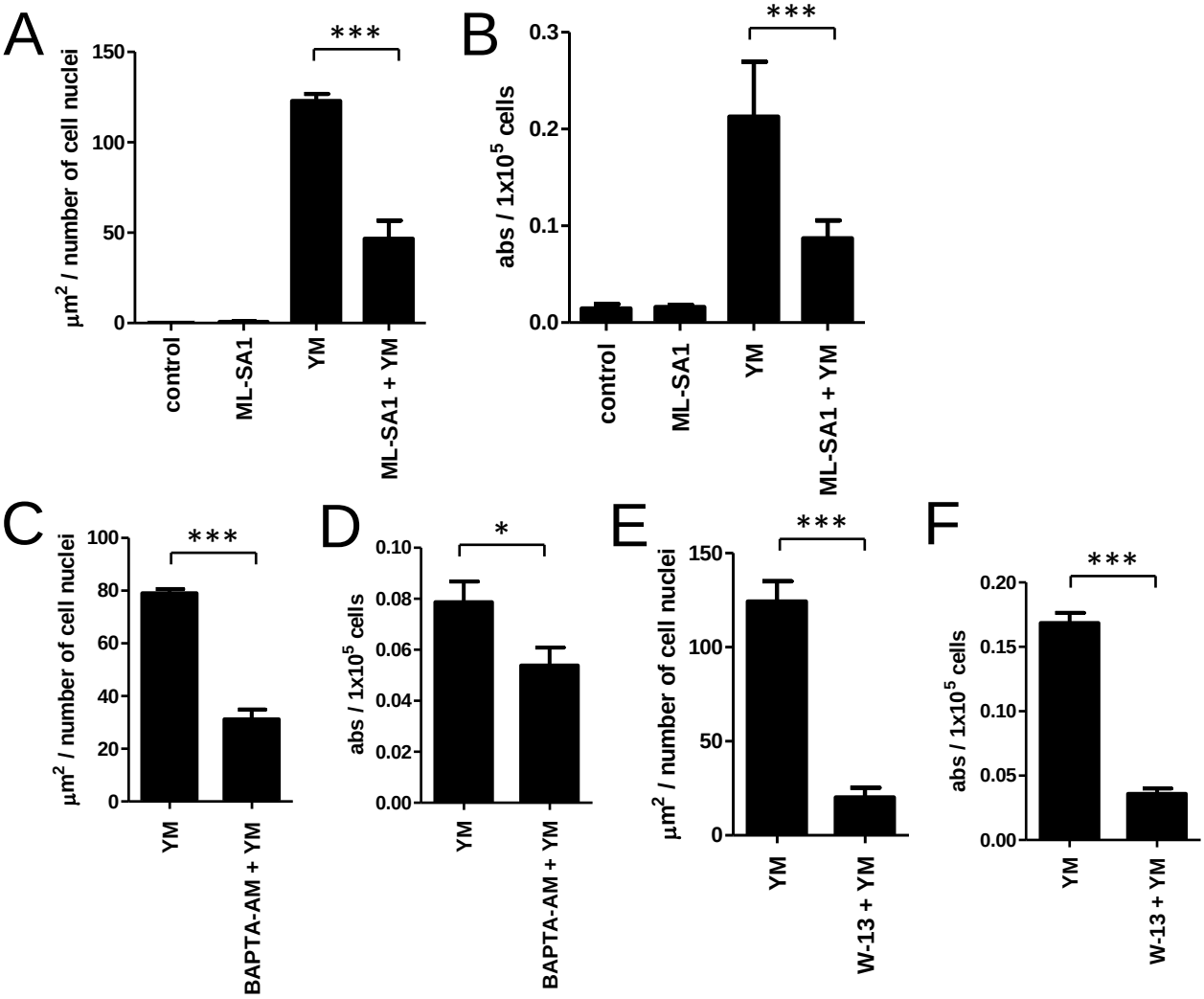
A
***
150
100
50
0
µm2 / number of cell nuclei
control
ML-SA1
YM
ML-SA1 + YM
B
***
0.3
0.2
0.1
0.0
abs / 1x105 cells
control
ML-SA1
YM
ML-SA1 + YM
C
***
100
80
60
40
20
0
µm2 / number of cell nuclei
YM
BAPTA-AM + YM
D
*
0.10
0.08
0.06
0.04
0.02
0.00
abs / 1x105 cells
YM
BAPTA-AM + YM
E
***
150
100
50
0
µm2 / number of cell nuclei
YM
W-13 + YM
F
***
0.20
0.15
0.10
0.05
0.00
abs / 1x105 cells
YM
W-13 + YM